

Numerical Study of the Mechanism of Laser Forming Process

K. PARAMASIVAN^{1,*}, S. DAS², S. MARIMUTHU³ AND D. MISRA³

¹*School of Laser Science & Engineering, Jadavpur University, Kolkata-700032, West Bengal, India*

²*Mechanical Engineering Department, Jadavpur University, Kolkata-700032, West Bengal, India*

³*Manufacturing Technology Centre, Coventry, CV7 9JU, UK*

This paper presents the mechanism of laser bending process. A finite element (FE) multiphysics modelling for the laser forming process of AISI 304 stainless steel is carried out to understand the deformation behaviour of the plate during the process. The temperature, stress and displacement distributions are captured at every single time interval on two mutually perpendicular cross-sectional planes (X-Z and Y-Z) of the plate for better elucidation of the ongoing process. COMSOL MULTIPHYSICS has been used to simulate the temperature distribution and deformation of sheet metal. The plate deformation during the process has been discussed in detail in the present work.

Keywords: Laser forming, AISI 304 stainless steel, numerical method, finite element (FE), temperature gradient mechanism (TGM), buckling mechanism (BM) upsetting mechanism (UM)

1 INTRODUCTION

Till now, the area of laser forming mostly deal with the study of the effects of primary and secondary laser parameters, laser irradiation strategy, dimensions of geometry on the final shape of the workpiece; however, few investigators have discussed about the mechanism of bending that determines final shape of the workpiece. Most of their results show that the final deformed shape can be either in the positive or negative z-direction and this depends on

*Corresponding author: E-mail: parma.gce@gmail.com

a number of factors including the process parameters. Until now, three main mechanisms have been discussed based on the bending direction of the work-piece caused by the temperature gradient through the thickness of plate [1-4].

When the plate undergoes deformation through the temperature gradient mechanism (TGM), it bends towards the laser beam (positive z -direction), whereas buckling mechanism (BM) generally introduces bending away from the laser beam (negative z -direction). In upsetting mechanism (UM), the plate is compressed with an almost constant strain along the thickness due to a nearly homogeneous temperature field across the plate thickness, causing a localised shortening and an increase of local thickness.

Wu *et al.* [5] studied laser bending process for borosilicate glass sheet. They have analysed the glass bending mechanism using TGM through the distribution of the temperature and thermal stress along the thickness direction. Jamil *et al.* [6] studied the TGM and BM laser bending mechanisms through the numerical investigation on forming of stainless steel sheets and tube. Li and Yao [7] examined the mechanisms of laser bending of tubes to figure out the deformation characteristics such as wall thickness variation, cross-section ovalization, bending radius and asymmetry. Chen and Zhang [8] conducted laser microbending process of Ti6Al4V square bar using a three-dimensional (3-D) thermo-mechanical finite element method (FEM) analytical model. Their results show that the radiation of the laser beam yields a rapid temperature increase at the irradiated surface, leading to the high temperature gradients between the irradiated surface and unirradiated surface, which suggests that the mechanism of laser micro bending is through temperature gradient mechanism. Pence *et al.* [9] studied the microforming process using shock waves induced by a nanosecond pulsed laser. They have conducted the various experimental and numerical investigations on aluminium sheets to study different mechanisms (positive or negative). Further, they developed correlation equations, through statistical method, for determination of bending angle as a function of laser process parameters for positive bending cases. Che Jamil *et al.* [10] investigated the effect of different beam geometries on laser bending process of metal sheets, which is dominated by the TGM, as did Lawrence *et al.* [11] with multimode laser beams. Shen [12] analysed the deformation mechanisms of the two-bridge actuator when applying a laser microadjustment. They have suggested that the in-plane (TGM), out-of-plane (TGM) and shortening (UM) deformation behaviour (coupling mechanism) in the two-bridge actuator are generated during laser microadjustment process. Shi *et al.* [13] studied the temperature gradient mechanism to obtain further insight into the deformation of a plate in the laser forming process. They have observed that under the processing conditions of TGM, the plate bends not only about the x -axis but also about the y -axis. Shi *et al.* [14] established a judgment criterion based on critical load $F_{buckling}$ which indicates the direction of bending for a sheet metal.

As can be seen from the literature, only a few researchers have attempted to investigate the mechanisms during laser bending process; however, their attempts are mostly based on experimental techniques, which may not pos-

sibly explore the underlying phenomenon, so much vividly and exhaustively, a numerical method can do. The purpose of the present work is to study the deformation behaviour of a plate through numerical simulation towards gaining a better insight into the corresponding mechanism.

2 FINITE ELEMENT (FE) SIMULATION OF THE LASER FORMING PROCESS

AISI 304 stainless steel sheet of $100 \times 50 \times 1.5 \text{ mm}^3$ was used to study the laser bending process. Simply-supported boundary conditions are applied at the fixed end of the plate, and the other end is kept free. The scanning path of laser beam passes through the middle of the plate along the y axis as shown in Figure 1. The governing equations for heat conduction within the specimen as well the equations of the structural model used for the description of the problem are taken [15] as they are incorporated in the commercial finite element (FE) software COMSOL Multiphysics.

The input parameters used were a laser power of 300 W, a scanning speed of 10 mm/s, a spot diameter of 2 mm and a plate thickness of 1.5 mm (along the z -axis). Figure 1 shows the schematic view of the geometry of workpiece and coordinate system. Initial temperature of the AISI 304 stainless steel plate was considered to be as 300 K.

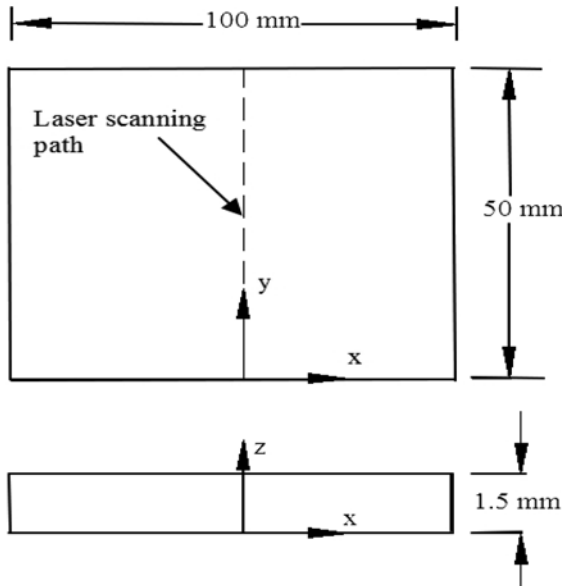


FIGURE 1
Schematic view of the geometry of the workpiece and coordinate system.

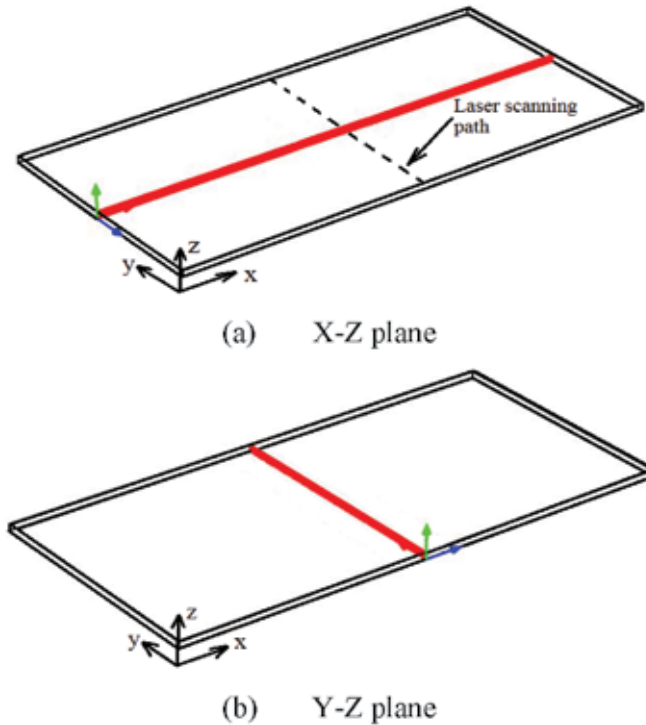


FIGURE 2
Cut-sections for monitoring of temperature, stress and displacement distributions.

To study the process of laser bending, two cross-sectional views of the workpiece are taken: one along the X-Z plane, across the scanning path, and the other along the Y-Z plane, passing through the scanning path. The cut-sections are shown in Figure 2). The temperature, stress and displacement distributions are captured in Figure 2(a) from the front view on the X-Z plane passing through the centre of the plate width, and in Figure 2(b) from the right side view on the Y-Z plane which crossing the centre of the plate length. The distributions are monitored on both cross sections during the period of irradiation cooling phase.

3 TRANSIENT TEMPERATURE, STRESS AND DEFORMATION FIELDS

3.1 Results overview

To elucidate the mechanism of bending process, the temperature, stress distributions and displacement fields on the X-Z plane at $y=25$ (half-way along the scan line) and Y-Z plane at $x=50$ (along the scan line) are presented at different time intervals covering Figure 3 through to Figure 26. The plate

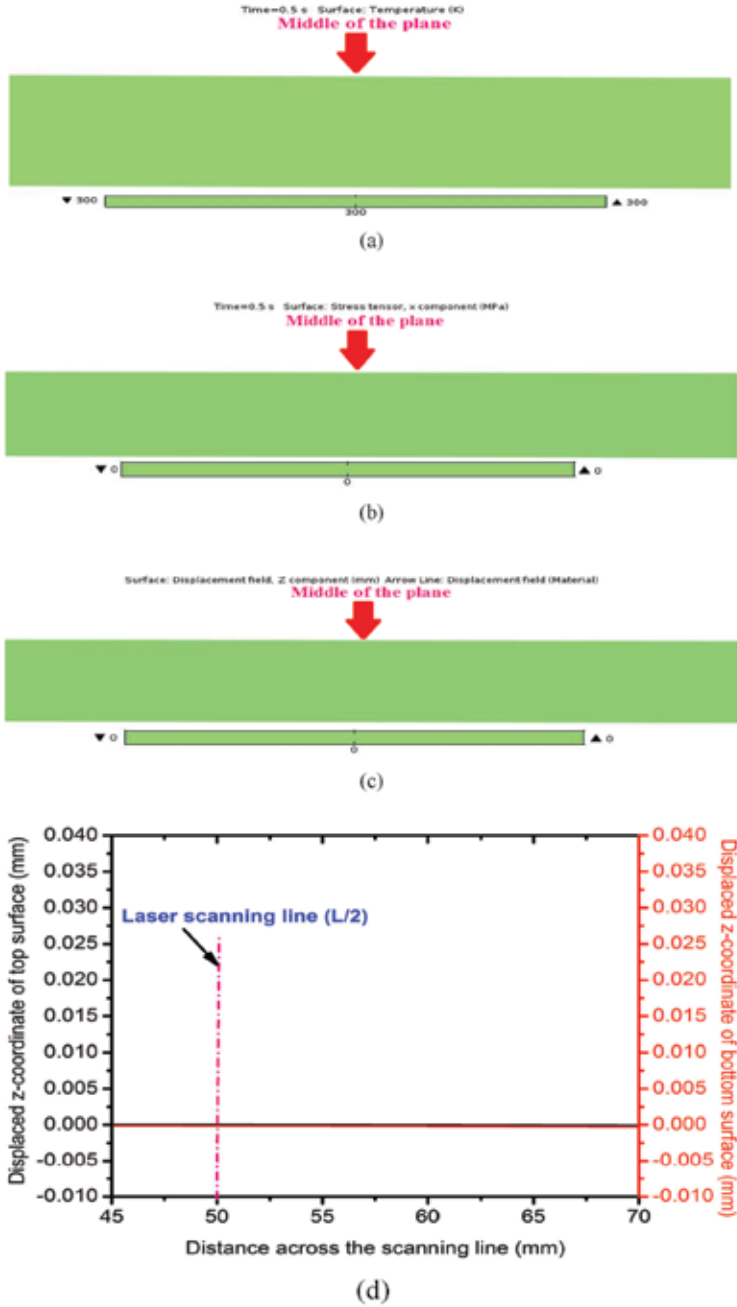


FIGURE 3 Images showing (a) temperature distribution, (b) x-component of stress, (c) z-component of displacement and (d) a graph showing displacement across the scanning line on the X-Z plane at $t=0.50$ seconds.

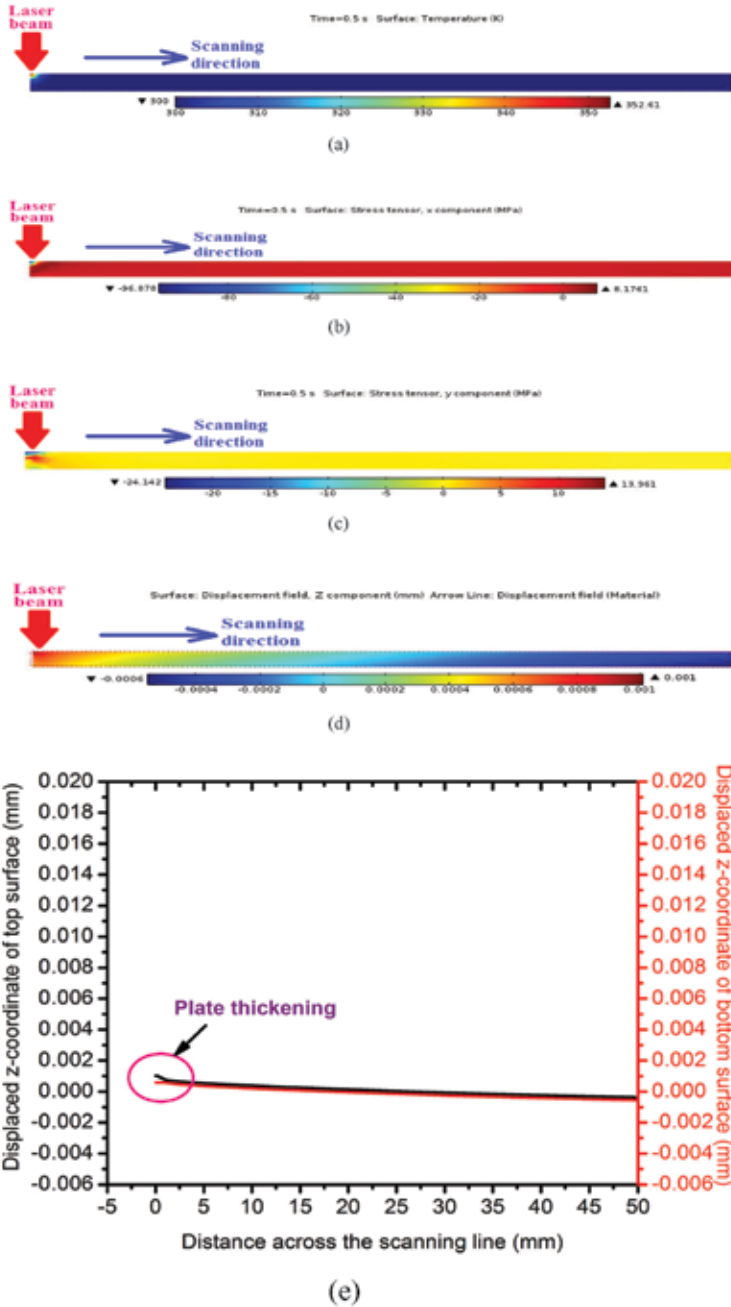


FIGURE 4 Images showing (a) temperature distribution, (b) x-component of stress, (c) y-component of stress, (d) z-component of displacement with nodal displacement vector and (e) a graph showing displacement across the scanning line on the Y-Z plane at t=0.50 seconds.

behaviour during the laser bending process has been studied during three vital stages. First, in order to observe the counter-bending at the early stage of heating, the distributions are monitored on both the selected planes. Next, the distributions and displacement fields are monitored while the laser beam is moving through the intermediate portion of the plate. Finally, the distributions and displacement fields are monitored while laser beam approaches the farthest edge of the plate and during the cooling phase. The displacement of nodes lying on the X-Z and Y-Z plane are presented with arrow plot (representing vector quantity) for better visualisation. The purpose of this plot is to understand the plate deformation direction and plate thickening during the heating process.

3.2 At $t=0.50$ seconds, when the laser beam just touches the starting edge of the plate

Figures 3(a) to (d) show the distributions on the X-Z plane when the laser beam just touches the starting edge of the plate. A small rise in temperature observed at the edge of the plate, as is evident in Figure 4(a), which represents the temperature distribution on the Y-Z plane. In Figure 3(d), the x -axis indicates the distance on the X-Z plane, left hand side y -axis indicates the z -displacement at the top surface of X-Z plane from initial state and right hand side y -axis indicates the z -displacement at the bottom surface of X-Z plane from initial state.

Figure 4(b) and Figure 4(c) show the x - and y -components of stress distribution on the Y-Z plane. The positive stress values representing the red region indicate tensile stresses, and the negative stress values represented by the blue region indicate compressive stresses. As can be seen from Figure 4(b) and Figure 4(c), when the laser beam approaches the starting end of the plate, it attains a compressive stress in the heated portion of the top surface and its neighbouring zone. Due to generation of heat and stress, the plate attains a slight displacement at the heated regions. It is clear from Figure 4(d), that the heated region moves towards the laser beam due to thermal expansion, so that, there is a local thickening at the plate top surface which can be seen from Figure 4(e). In Figure 4(e) the x -axis of this graph indicates the distance on the Y-Z plane and y axis indicates the z -displacement at the top and bottom surface of Y-Z plane.

3.3 At $t=0.60$ seconds, when half of the laser beam has entered into the plate

Still, there is no temperature and stress development on the X-Z plane, as shown in Figure 5(a), which is far away from the heated zone; nevertheless, the plate experiences counter-bending as can be seen from Figure 5 (d).

Figures 6(a) to (d) show the distributions on the Y-Z plane. As observed from Figure 6(a), that the plate has attained a maximum temperature of 1028 K at the top surface, but the temperature at bottom surface does not change much

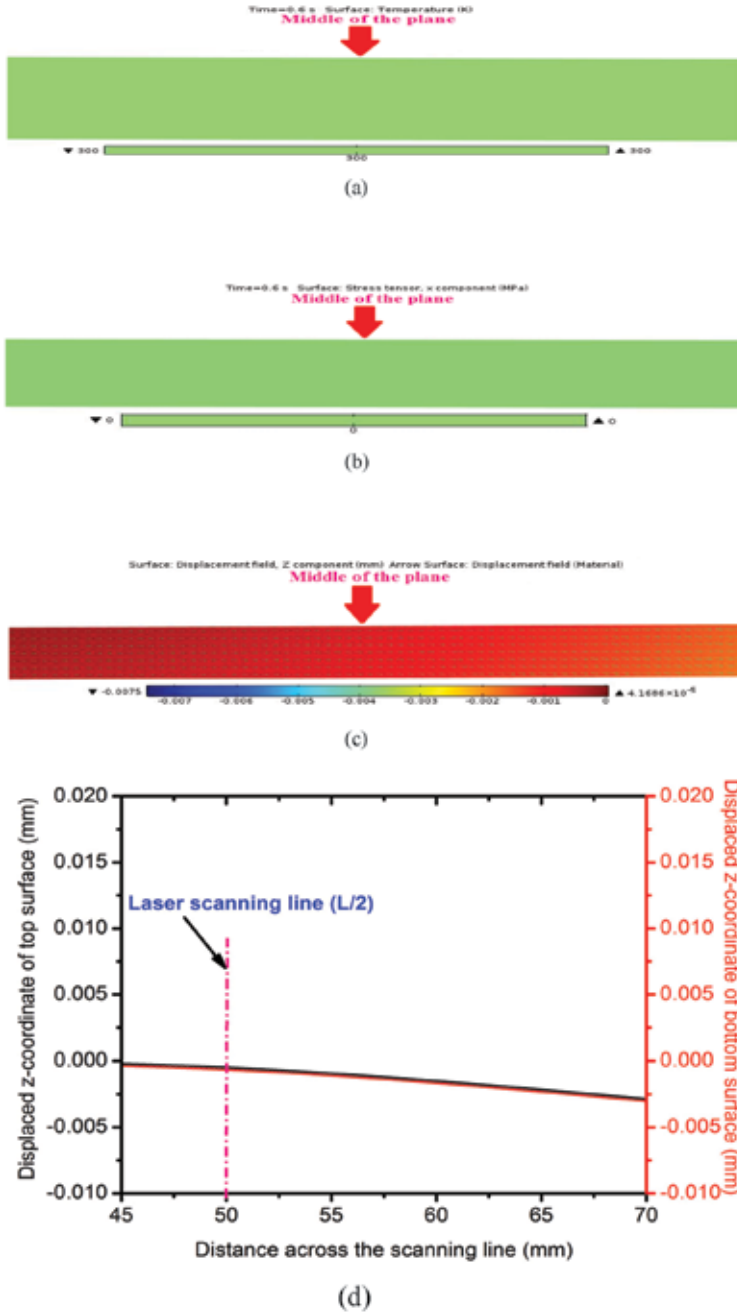


FIGURE 5

Images showing (a) temperature distribution, (b) x -component of stress, (c) z -component of displacement with nodal displacement vector and (d) a graph showing displacement across the scanning line on the X-Z plane at $t=0.60$ seconds.

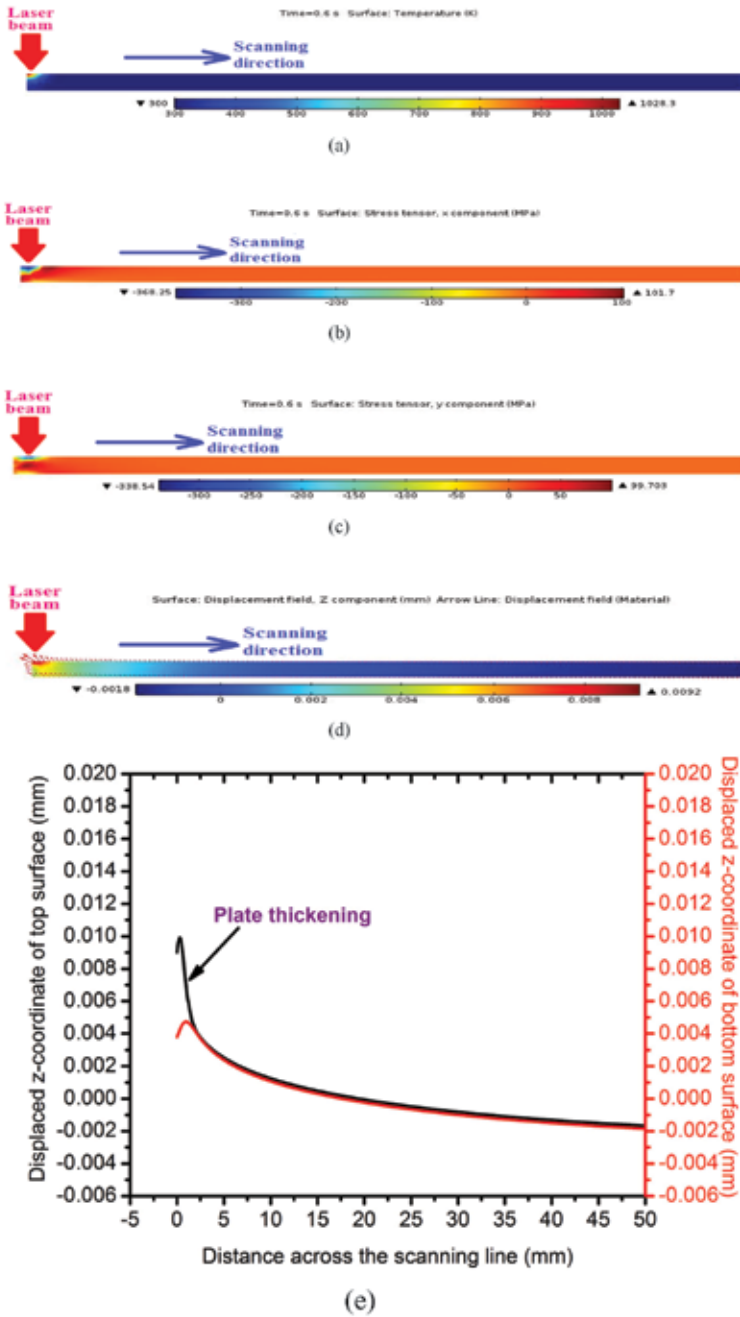


FIGURE 6 Images showing (a) temperature distribution, (b) x-component of stress, (c) y-component of stress, (d) z-component of displacement with nodal displacement vector and (e) a graph showing displacement across the scanning line on the Y-Z plane at $t=0.60$ seconds.

because it takes time for heat to penetrate through the total thickness of the plate. Due to this large temperature gradient along the direction of plate thickness, a high compressive and tensile stresses develop at the upper heated region and its neighbourhood, respectively, as can be seen from Figure 6(b) and Figure 6(c). It is clear from Figure 6(d), that the top and bottom surface of the heated region moves along a direction comprised of backward (-ve Y-axis) and upward (+ve Z-axis) directions. It is also noted that local thickening of the plate takes place which can be seen from Figure 6(d) and Figure 6(e).

3.4 At $t=0.70$ seconds, when half of the laser beam is fully inside the plate

It is observed from Figure 7(a) that there is no change in temperature; however, the top surface of X-Z plane attains a small amount of tensile stress due to counter bending as can be seen from Figure 7(c). The bottom surface of X-Z plane develops a compressive stress. As shown in Figure 7(c), at this time, the plate experiences a displacement towards +ve x -direction and downward direction of z -axis as well. The magnitude of counter-bending (about $6.7 \mu\text{m}$) involved at this time can be seen from Figure 7(d).

Distributions and z -component of displacement on the Y-Z plane are shown in Figures 8(a) to (d). Figure 8(a) indicates that the temperature at the top heated surface increases further and it is propagating to the surrounding zone through conduction. Figure 8(d) and Figure 8(e) illustrate that due to further rise in temperature and stresses at the heated and surrounding region, the plate attains additional bulging at the heated region and plate displacement occurs towards to the negative direction of laser irradiation (-ve Y-axis).

3.5 At $t=0.80$ seconds, when the centre of the laser beam is at (50.0, 2.0, 1.5)

As shown in Figures 9(a) to (c), there is not much change in temperature, stress and displacement on the X-Z plane compared to the time step at $t=0.7$ seconds discussed above. It is noticed, however, from Figure 9(d) that the plate has started to bend towards to the laser beam.

It is observed from Y-Z plane that when the laser beam approaches the point, the heated region of the plate develops further amount of compressive stress due to thermal expansion of a deeper and wider zone surrounding the beam. It is also noted that the compressive stress starts to decrease at the heated region of the plate due to rapid cooling of the region, and it changes to tensile stress from compressive due to the contraction of the material. Thickening of the plate and changes in plate dimension (width-wise) produced by local heating are shown in Figure 10(d) and Figure 10(e).

3.6 At $t=1.50$ seconds, when the centre of the laser beam is at (50.0, 9.0, 1.5)

It is noticed from Figure 11(a) that there is still no change in temperature at the X-Z plane corresponding to $y=25$ mm. But from Figure 11(b), it is evident that the top and bottom surfaces of the plate along the X-Z plane undergo small

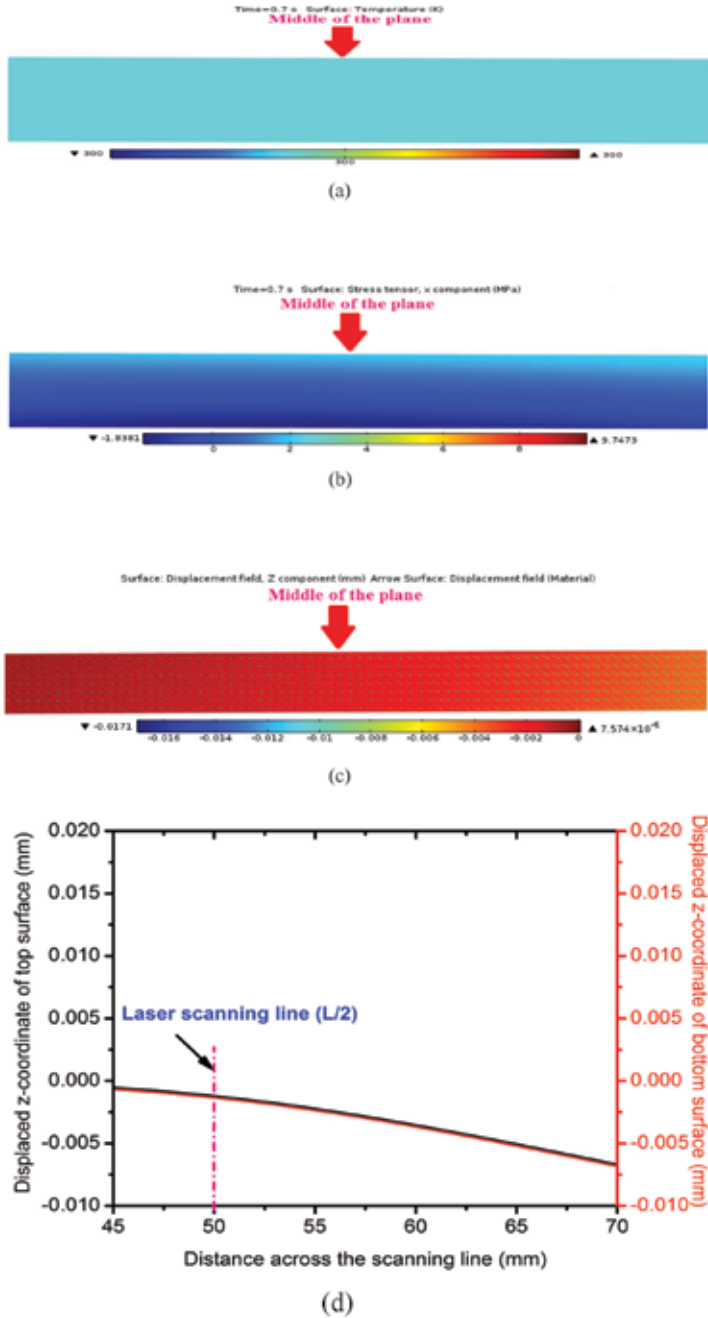


FIGURE 7 Images showing (a) temperature distribution, (b) x-component of stress, (c) z-component of displacement with nodal displacement vector and (d) a graph showing displacement across the scanning line on the X-Z plane at t=0.70 seconds.

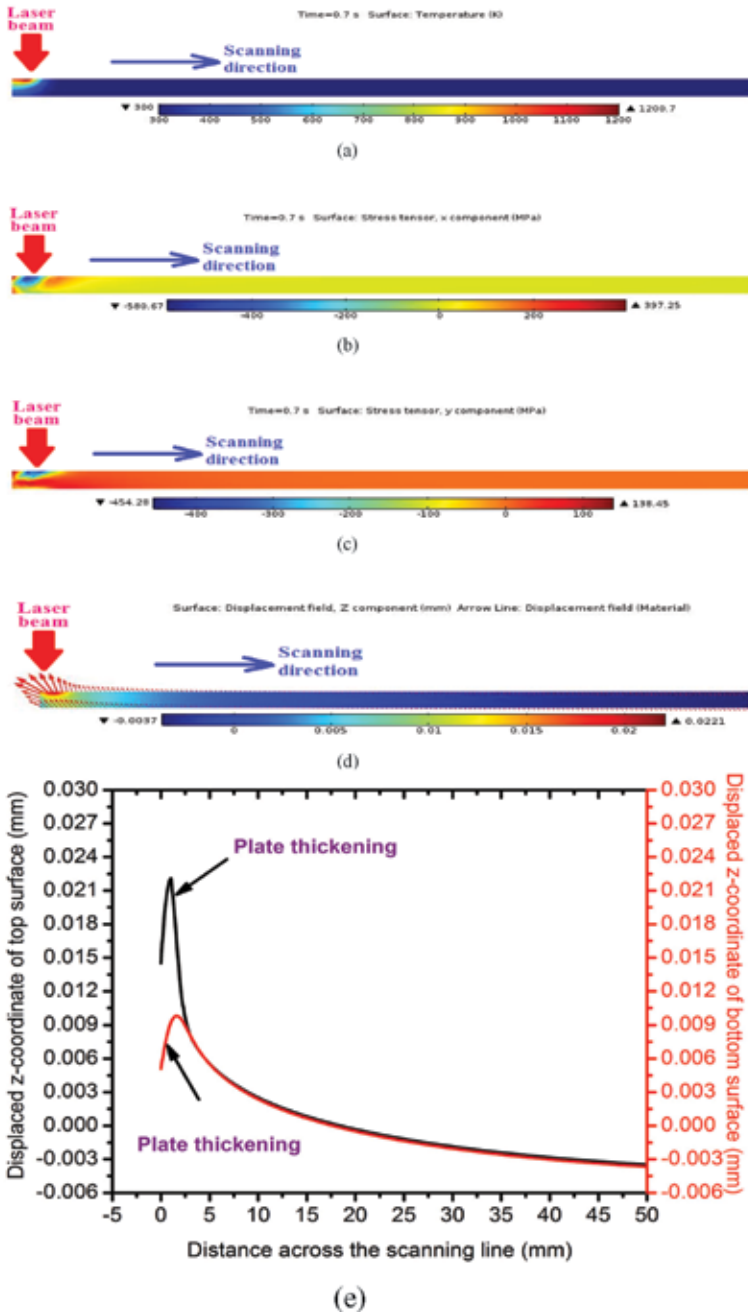


FIGURE 8

Images showing (a) temperature distribution, (b) x -component of stress, (c) y -component of stress, (d) z -component of displacement with nodal displacement vector and (e) a graph showing displacement across the scanning line on the Y - Z plane at $t=0.70$ seconds.

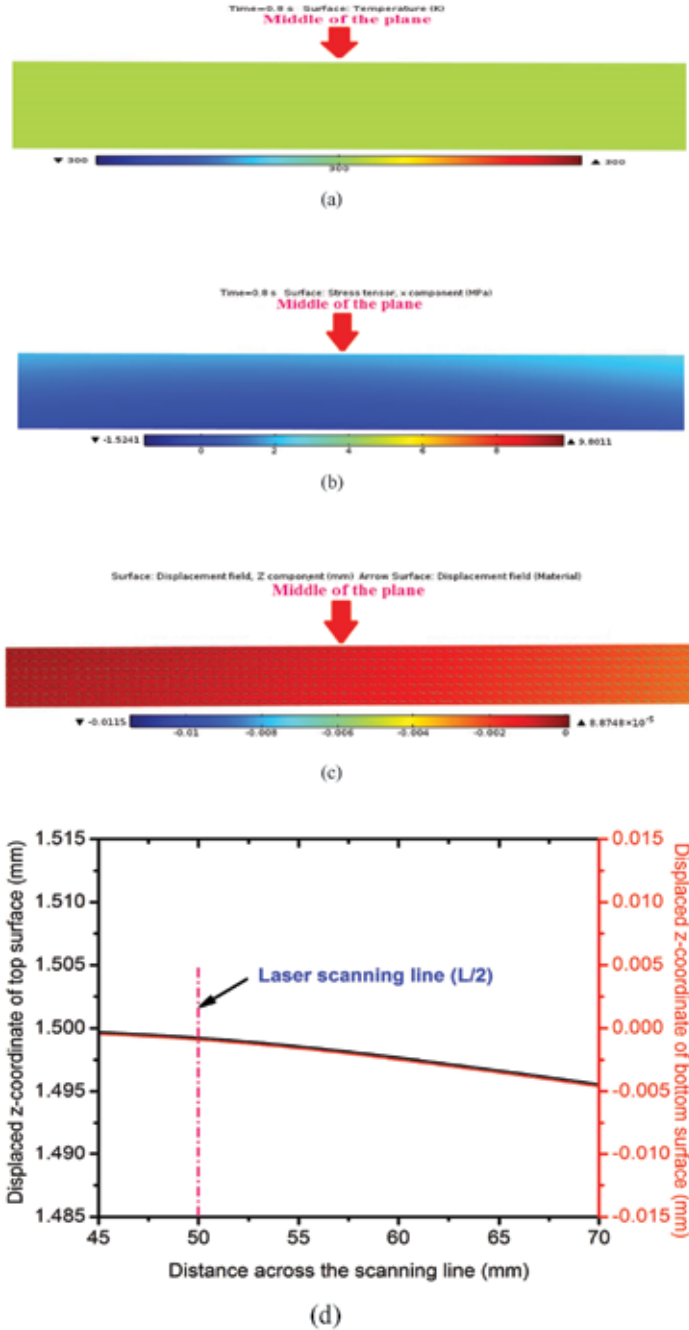


FIGURE 9 Images showing (a) temperature distribution, (b) x-component of stress, (c) z-component of displacement with nodal displacement vector and (d) a graph showing displacement across the scanning line on the X-Z plane at t=0.80 seconds.

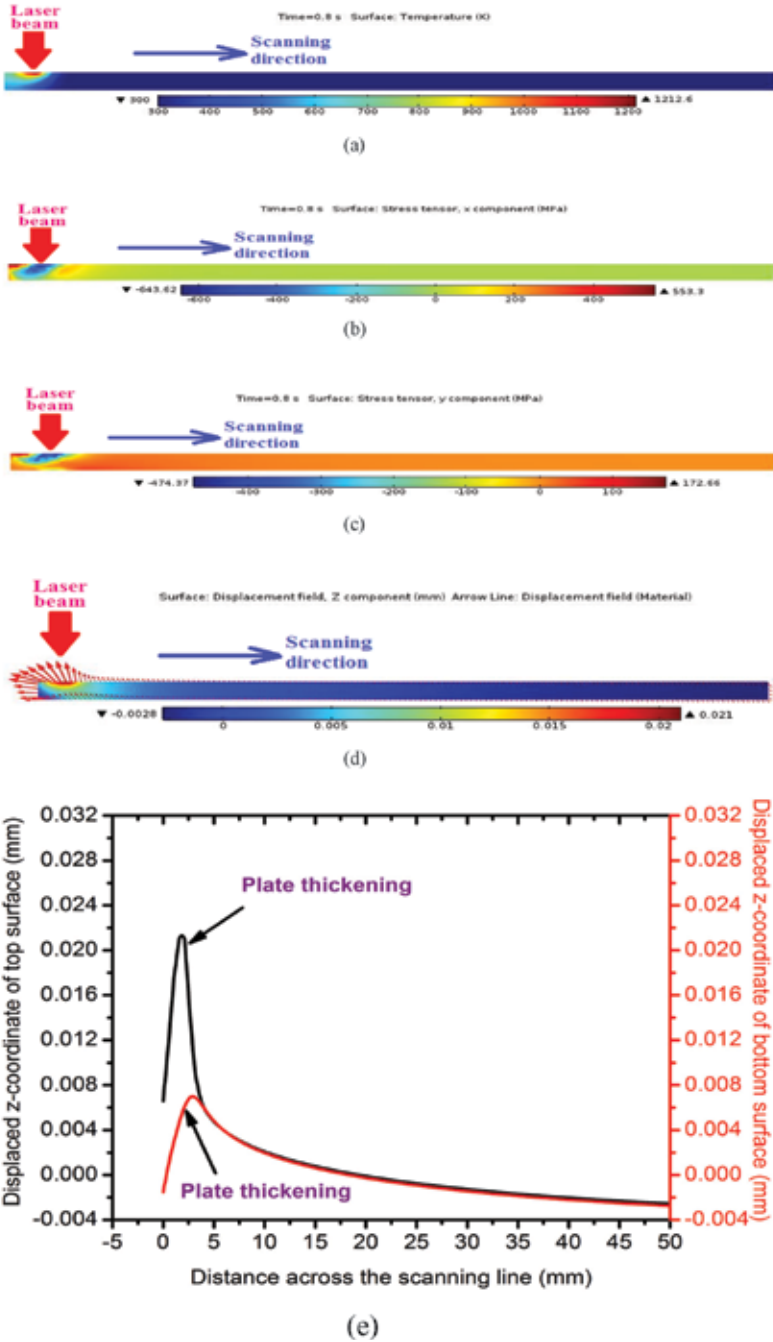


FIGURE 10

Images showing (a) temperature distribution, (b) x -component of stress, (c) y -component of stress, (d) z -component of displacement with nodal displacement vector and (e) a graph showing displacement across the scanning line on the Y - Z plane at $t=0.80$ seconds.

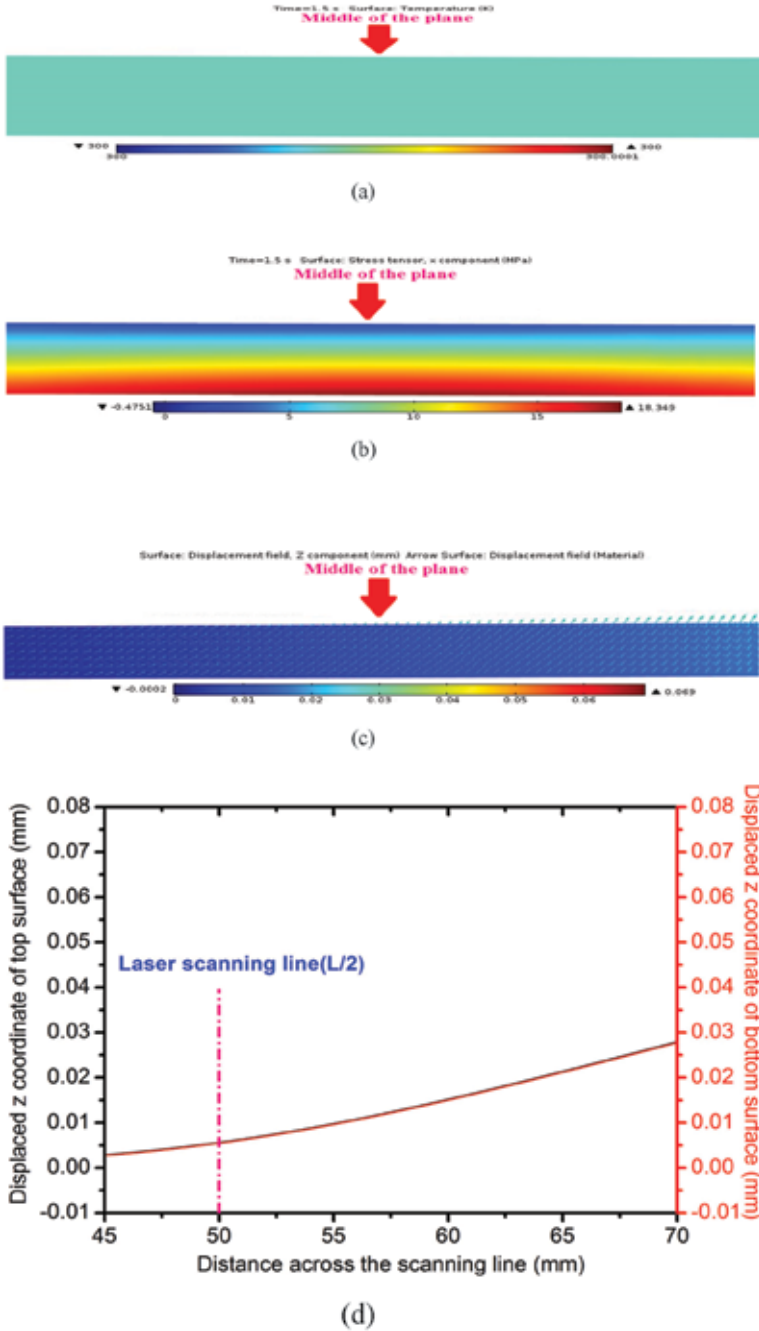


FIGURE 11 Images showing (a) temperature distribution, (b) x-component of stress, (c) z-component of displacement with nodal displacement vector and (d) a graph showing displacement across the scanning line on the X-Z plane at t=1.50 seconds.

amount of tensile stresses due to plate bending towards to the laser beam which can be seen from Figure 11(c). The extent of bending involved across the scanning path at this time can be seen from Figure 11(d) through the displaced position of the top and bottom surfaces along X-Z plane at $y=25$ mm.

The obtained distributions on the Y-Z plane for $t=1.50$ seconds are shown in Figures 12(a) to (e). It is observed that the laser beam induces a region of compressive stress at the heated region due to thermal expansion and trailing part of the heated regions experiences tensile stress due to rapid cooling of the region. Figure 12(d) and Figure 12(e) show z -displacement along the scanning path with thickening of plate and increment in length of the plate due to local heating.

3.7 At $t = 2.68$ seconds, when the centre of the laser beam is at (50.0, 20.8, 1.5)

As can be seen in Figures 13(a) to (d), temperature, stress and displacement have started to rise further when the laser beam moves close to the selected X-Z plane. During this time, the laser beam has travelled nearly half of the width of the plate, so that temperature attains a steady maximum by this time which can be seen from Figure 14(a). For this reason, the displacement of the plate gradually increases in the z -direction and also it moves towards the +ve x -direction during the laser heating phase as shown in Figure 13(c) and Figure 13(d); moreover, the tensile stress at the bottom surface of X-Z plane increases rapidly (in terms of magnitude and spread of volume). Comparing Figure 11(b) corresponding to $t=1.50$ seconds and Figure 13(b) at $t=2.68$ seconds, it can observe tensile stress increases from about 18 MPa to about 148 MPa. This rapid rise in tensile stress leads to an increase in plate displacement in z -direction.

Distributions on the Y-Z plane are shown in Figures 14(a) to (e). As is clear in Figure 14(a), the large temperature difference (gradient) between the top and bottom of Y-Z plane is observed which is indicative of bending through temperature gradient mechanism. As shown in Figure 14(b) and Figure 14(c), the plate experiences a high compressive stress along the longitudinal and transverse directions on the Y-Z plane.

Comparing Figure 14(b) and Figure 14(c) shows that the compressive stress maximum of 613 MPa is observed along the longitudinal direction of the Y-Z plane, whereas the compressive stress maximum of 460 MPa is attained along the transverse direction of the Y-Z plane. That is why the plate moves towards +ve x -direction and +ve z -direction as shown in Figure 14(d). The plate thickening caused by local heating is shown in Figure 14(e).

3.8 At $t=2.98$ seconds, when the centre of the laser beam is at (50.0, 23.8, 1.5)

As shown in Figure 15(a), temperature starts to rise rapidly at the top surface of X-Z plane due to conduction so that the top surface of X-Z plane alters

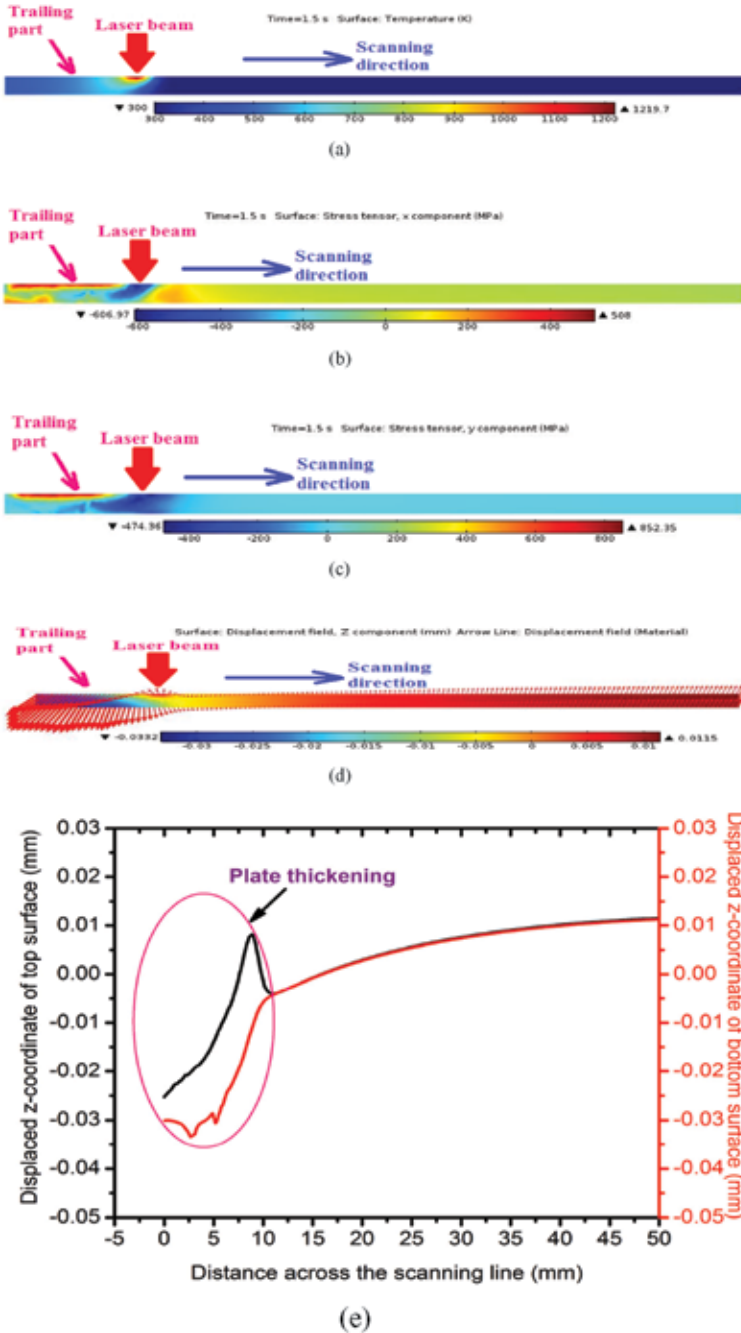


FIGURE 12

Images showing (a) temperature distribution, (b) x-component of stress, (c) y-component of stress, (d) z-component of displacement with nodal displacement vector and (e) a graph showing displacement across the scanning line on the Y-Z plane at t=1.50 seconds.

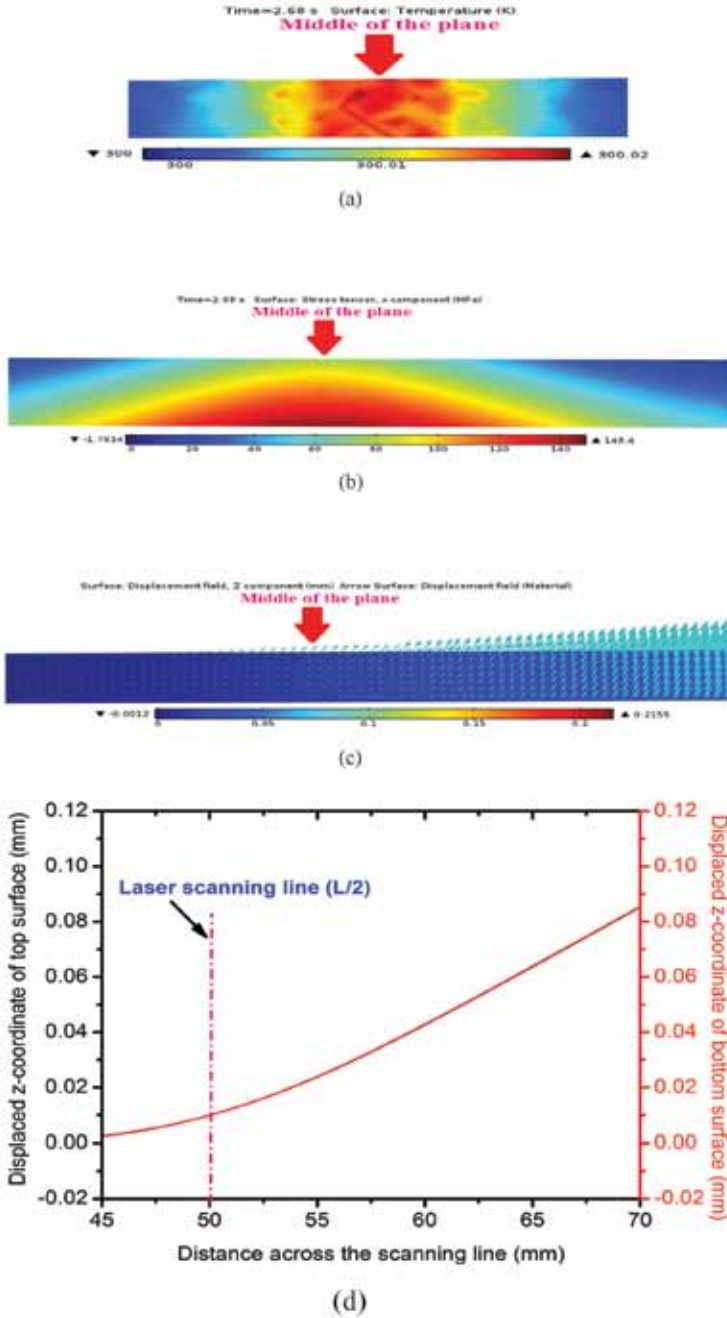


FIGURE 13

Images showing (a) temperature distribution, (b) x -component of stress, (c) z -component of displacement with nodal displacement vector and (d) a graph showing displacement across the scanning line on the X - Z plane at $t=2.68$ seconds.

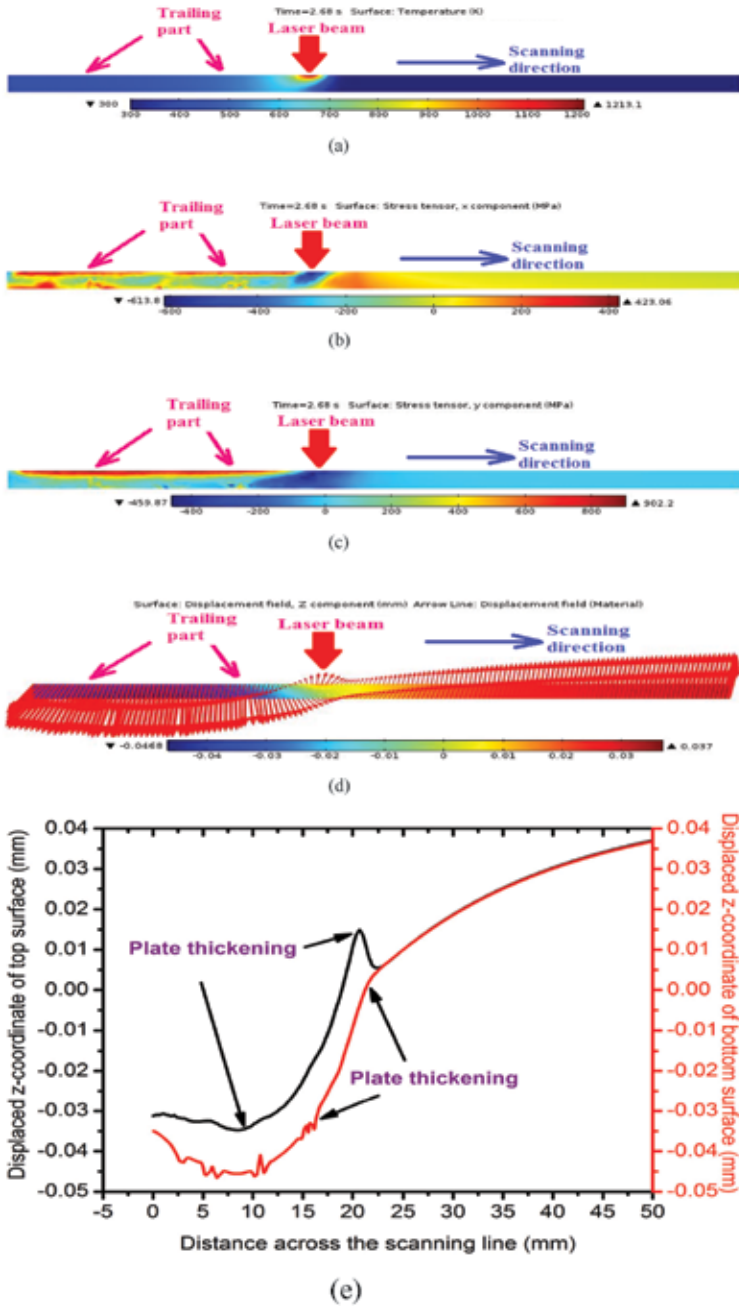


FIGURE 14

Images showing (a) temperature distribution, (b) x -component of stress, (c) y -component of stress, (d) z -component of displacement with nodal displacement vector and (e) a graph showing displacement across the scanning line on the Y - Z plane at $t = 2.68$ seconds.

from tensile to compressive stress due to thermal expansion of the zone surrounding the beam. It is also noted that the bottom surface of the tensile stress on the X-Z plane starts to decline due to the temperature gradient along the plate thickness.

The amount of tensile stress reduction in the bottom surface of the X-Z plane can be seen by comparing Figure 15(b) and Figure 13(b). The plate z-displacement along with plate thickening is shown in Figure 15(c) and Figure 15(d). Due to effect of conduction, the selected X-Z plane is preheated even before laser beam reaches the X-Z plane. Therefore, the top surface of the X-Z plane attains a bulging. Figures 16(a) to (e) show the distributions on the Y-Z plane.

3.9 At $t=3.12$ seconds, when the centre of the beam reaches the top surface of the X-Z plane

The temperature attains a maximum when the centre of the laser beam reaches the top surface of the X-Z plane, as shown Figure 17(a). Figure 17(b) shows the x -component of stress distribution corresponding to the temperature distribution (*cf.* Figure 17(a)), where the maximum compressive stress is produced at the top surface of X-Z plane due to the occurrence of maximum temperature. At this time, the compressive stress of 200 MPa develops at the bottom surface of the X-Z plane due to increment in temperature at the bottom surface of the X-Z plane. It is also shown that the induced stress gradient through the plate thickness which occurs due to thermal expansion of the material in the heated zone.

Figure 17(c) reveals that the z -displacement across the scanning path with the plate thickening produced by local heating. As can be seen in Figure 17(c) and Figure 17(d) that plate thickening occurred only at the laser scanning path, and there is no uneven thickening at the regions towards to the free end of the plate.

Temperature and stress distributions and z -displacement of the top and bottom surface along the scanning line on the Y-Z plane are presented in Figures 18(a) to (e).

3.10 At $t=3.24$ seconds, when the laser beam moves away from the X-Z plane

During this period of time (at $t=3.24$ seconds), the centre of the laser beam is at (50.0, 26.4, 1.5). As shown in Figure 19(a), when the laser beam moves away from the X-Z plane, the temperature starts decreasing due to rapid cooling of the region. For this reason, the compressive stress at the top surface of X-Z plane starts decreasing and it changes to tensile stress on account of contraction of the surrounding material.

Figure 19(c) and Figure 19(d) indicate the z -displacement of the X-Z plane. As can be seen in Figure 19(c) and Figure 19(d), the bottom surface of

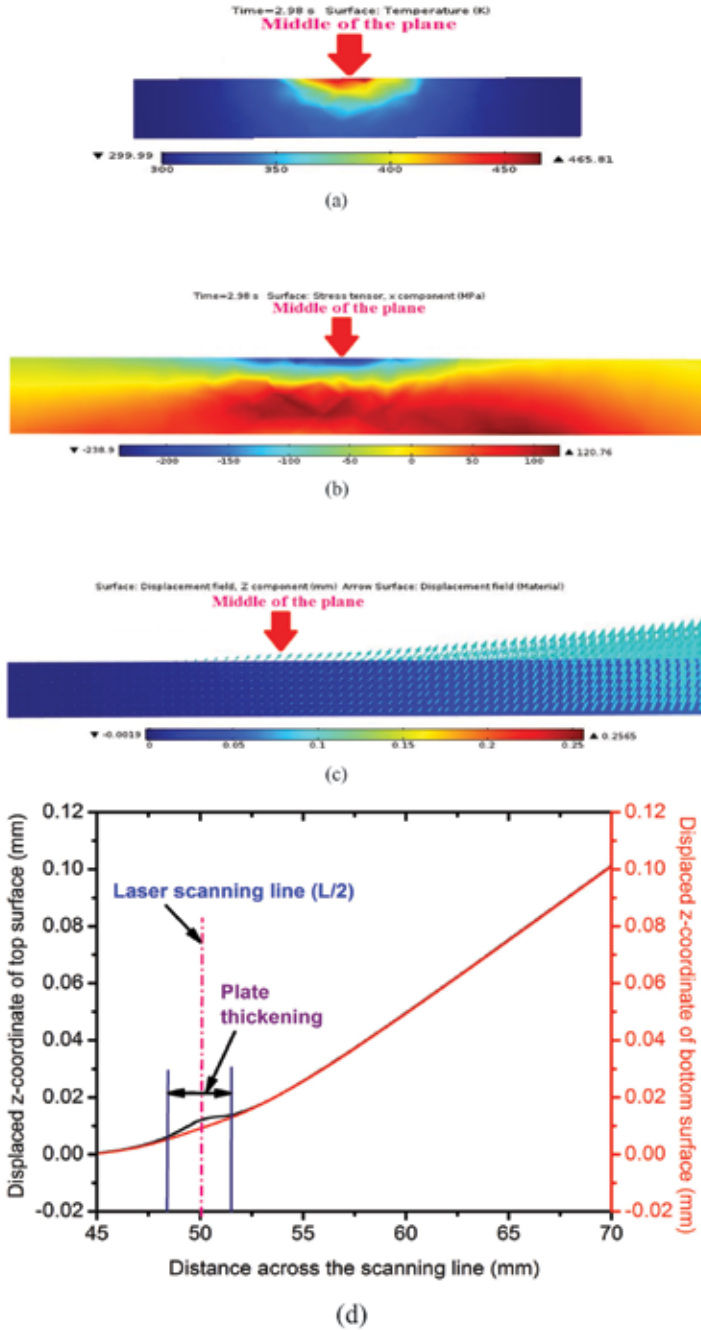


FIGURE 15

Images showing (a) temperature distribution, (b) x-component of stress, (c) z-component of displacement with nodal displacement vector and (d) a graph showing displacement across the scanning line on the X-Z plane at $t=2.98$ seconds.

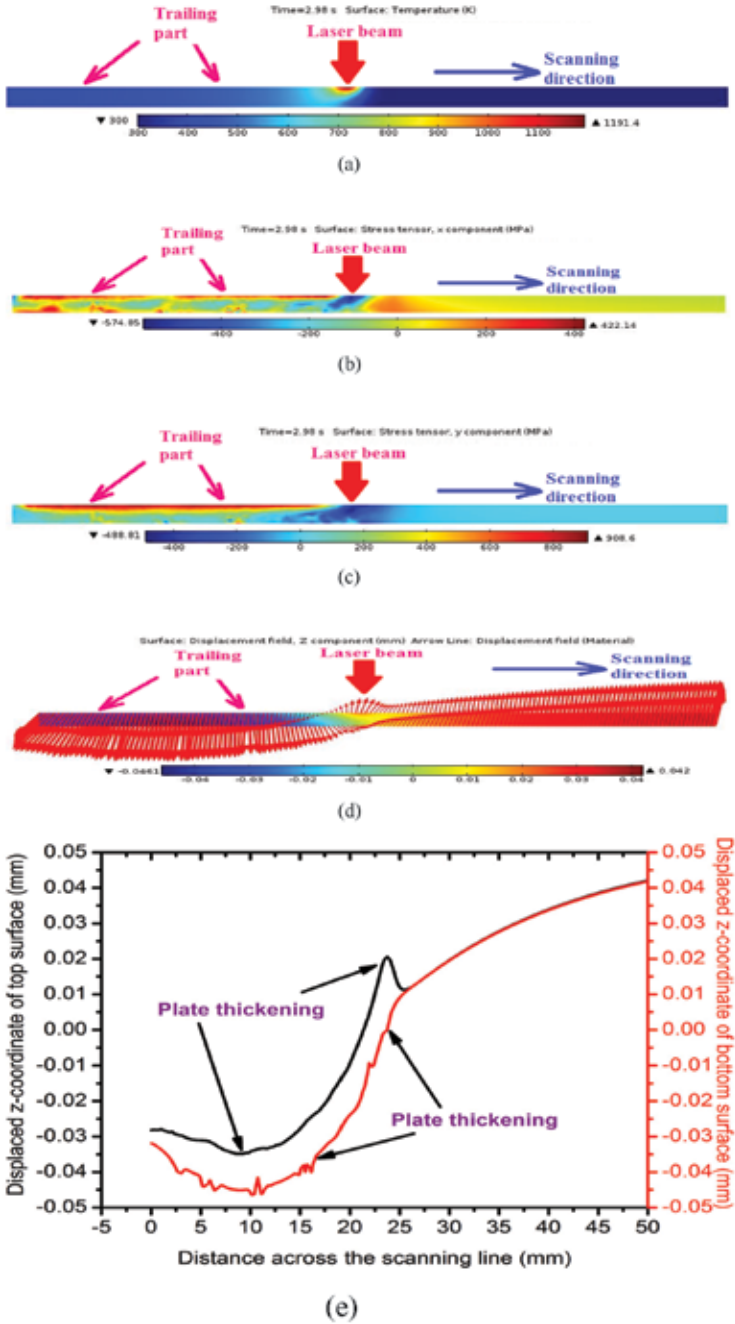


FIGURE 16

Images showing (a) temperature distribution, (b) x-component of stress, (c) y-component of stress, (d) z-component of displacement with nodal displacement vector and (e) a graph showing displaced displacement across the scanning line on the Y-Z plane at $t=2.98$ seconds.

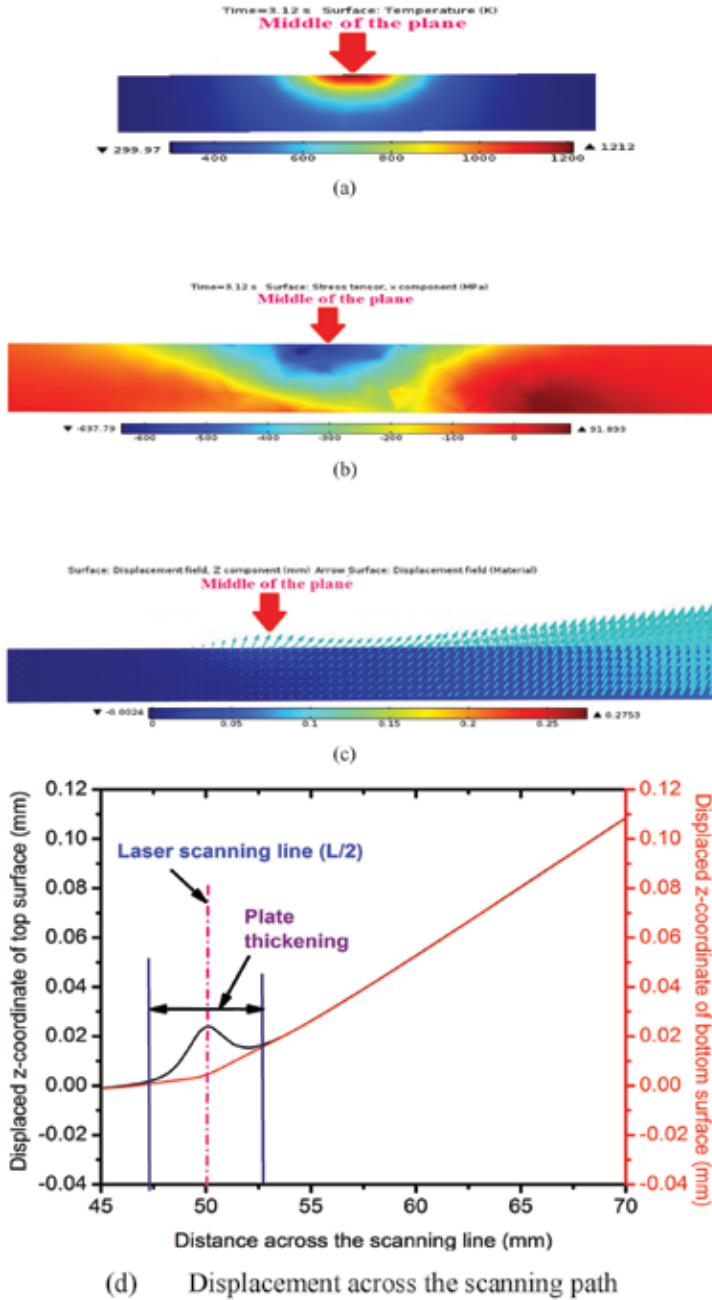


FIGURE 17

Images showing (a) temperature distribution, (b) x-component of stress, (c) z-component of displacement with nodal displacement vector and (d) a graph showing displacement across the scanning line on the X-Z plane at $t=3.12$ seconds.

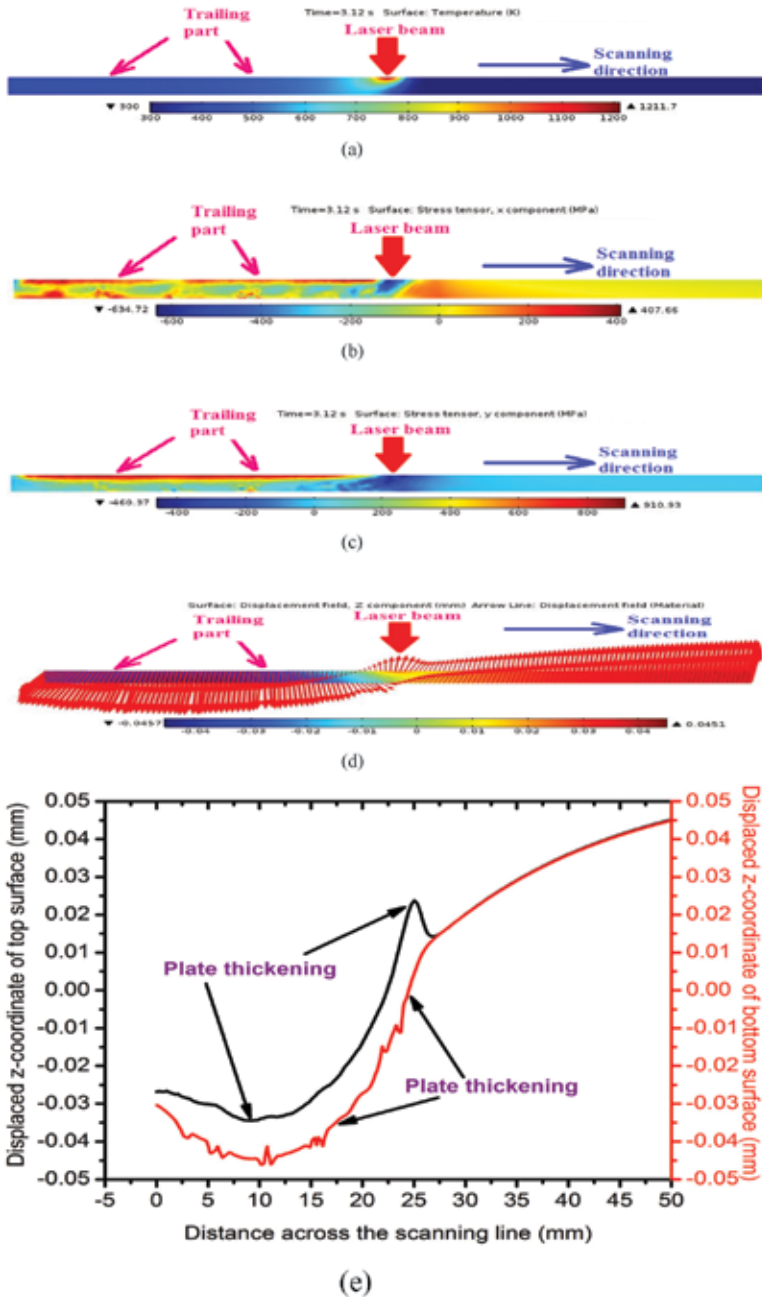


FIGURE 18

Images showing (a) temperature distribution, (b) x -component of stress, (c) y -component of stress, (d) z -component of displacement with nodal displacement vector and (e) a graph showing displacement across the scanning line on the Y-Z plane at $t=3.12$ seconds.

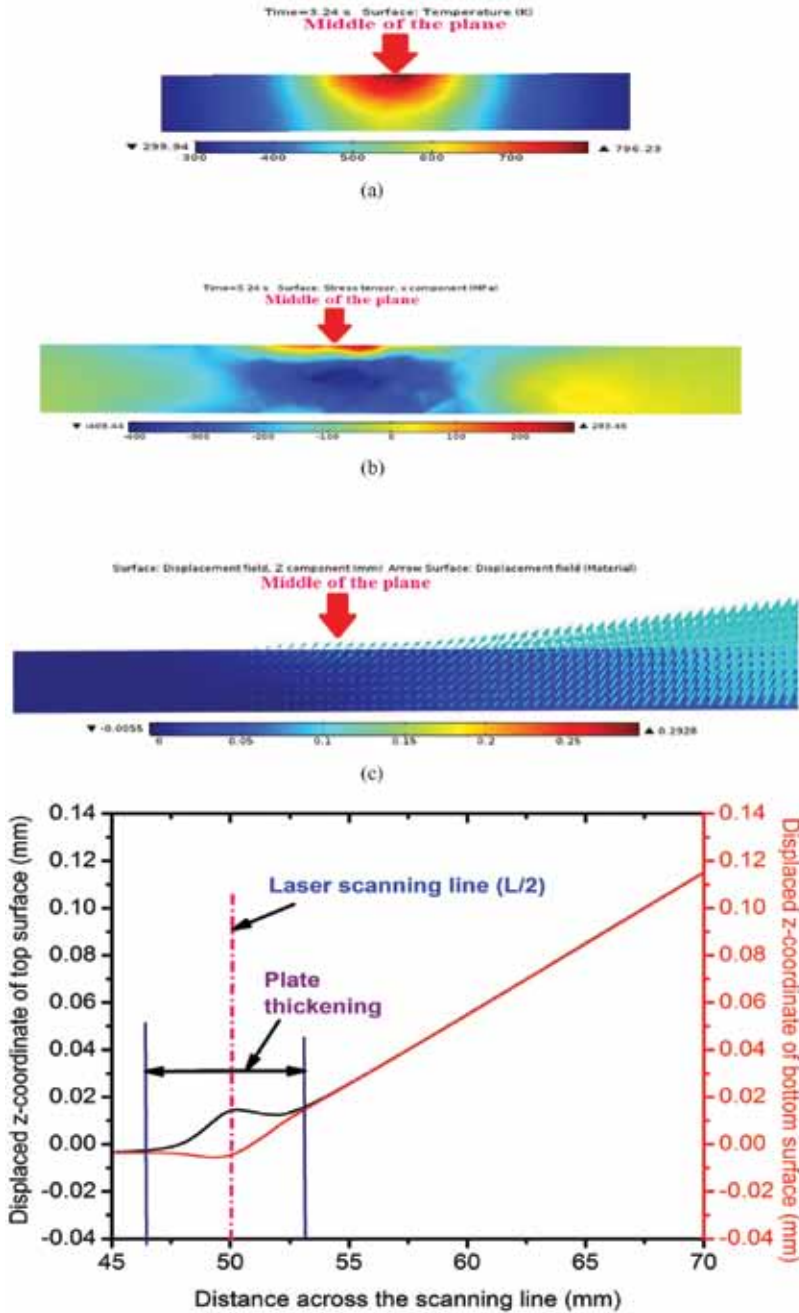


FIGURE 19

Images showing (a) temperature distribution, (b) x-component of stress, (c) z-component of displacement with nodal displacement vector and (d) a graph showing displacement across the scanning line on the X-Z plane at $t=3.24$ seconds.

X-Z plane attains a bulging but it takes place a little bit delayed due to the time taken by heat to flow through the plate thickness. The distributions for Y-Z plane is shown in Figures 20(a) to (e).

3.11 At $t=3.88$ seconds, when the centre of the beam leaves further away from the X-Z plane

It is noticed from Figure 21(a) that when the laser beam moves further away from the X-Z plane, the temperature decrease rapidly towards to the ambient temperature due to rapid cooling of the region, and it is also noticed that the temperature gradient along the plate thickness attains almost zero. As the temperature of the plate decreases, resulting in the stresses at the top and bottom surface of the plate starts to rise as tensile. Figures 22(a) to (e) show the temperature, stress and displacement distributions on the Y-Z plane at $t=3.88$ seconds. Figure 22(d) and Figure 22(e) show the plate bulging along the scanning path and changes in plate geometry.

3.12 At $t=5.60$ seconds, when the centre of the laser beam is at farthest edge of the plate

It is seen from what has gone before that the temperature and stresses of X-Z plane decreases further due to cooling. As shown in Figure 23, a much higher temperature is obtained at the end of the scan line compared to that at the beginning as well as that at the middle portion of the plate. The reason for this is that heat from the incident laser beam and the heat stored by the material behind the beam flows into the cold region ahead of the beam. As the beam reaches the edge, the heat flowing ahead of the beam cannot travel further and, consequently, a heat build-up occurs near the farthest edge of the plate. As the temperature of the plate increases, this results in higher compressive stresses, which can be seen from Figure 24(b). The plate geometry also alters towards to the scanning line direction (+ve Y-axis) when the laser beam is heating at the farthest edge of the plate, as shown in Figure 24(d). Figure 24(e) shows the plate thickening along the scanning line produced by laser irradiation.

3.13 At t approximately 60 seconds, after the cooling phase

It is seen from what has gone before that the temperature on the X-Z plane decreases near to ambient after sufficient time to cool the plate. As a result, the tensile stress at the top and bottom surfaces on the X-Z plane increases. Meanwhile, the compressive stress on the X-Z plane also decreases, which can be seen from Figure 25(b). Figure 25(c) and Figure 25(d) show the z -component of displacement of the top and bottom surface of X-Z plane.

As we know that the temperature starts rising rapidly when the laser beam approaches the beginning edge of the plate. Afterwards, the temperature reaches a steady until the beam approaches the farthest edge of the plate. Dur-

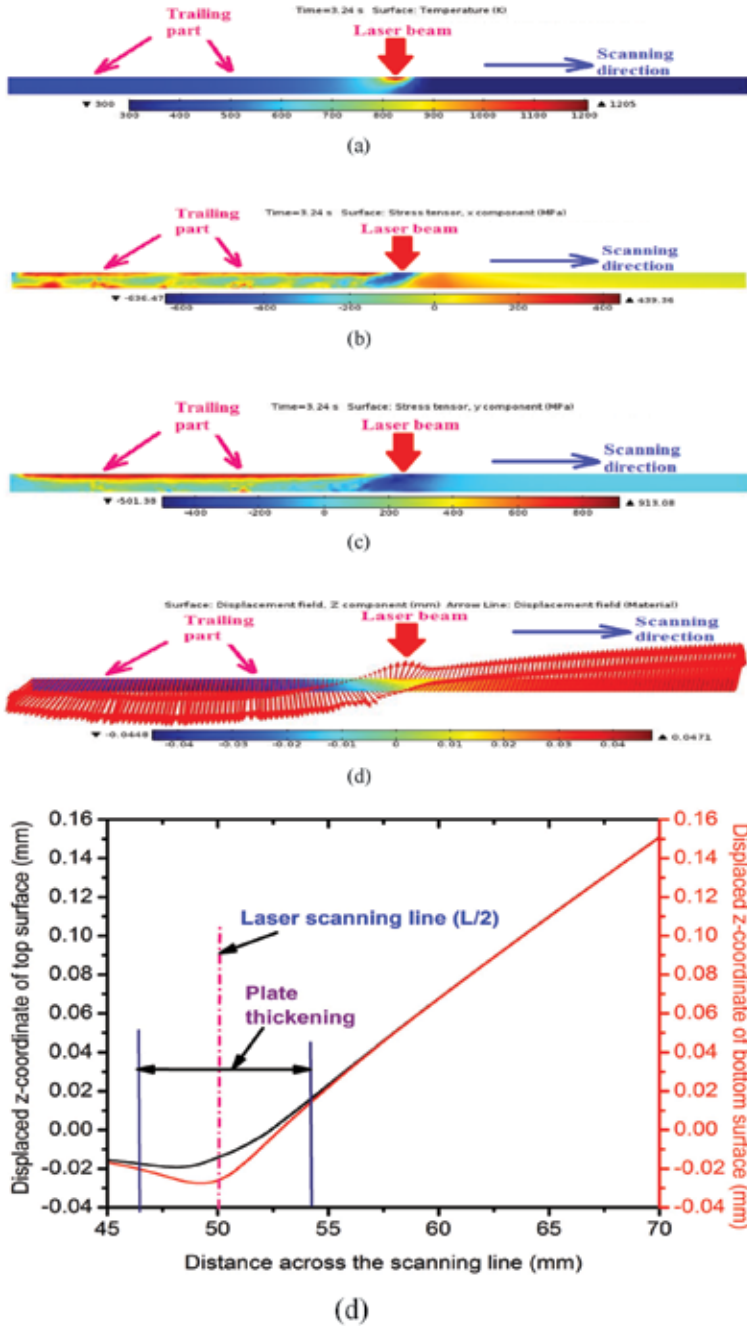


FIGURE 20

Images showing (a) temperature distribution, (b) x-component of stress, (c) y-component of stress, (d) z-component of displacement with nodal displacement vector and (e) a graph showing displacement across the scanning line on the Y-Z plane at $t=3.24$ seconds.

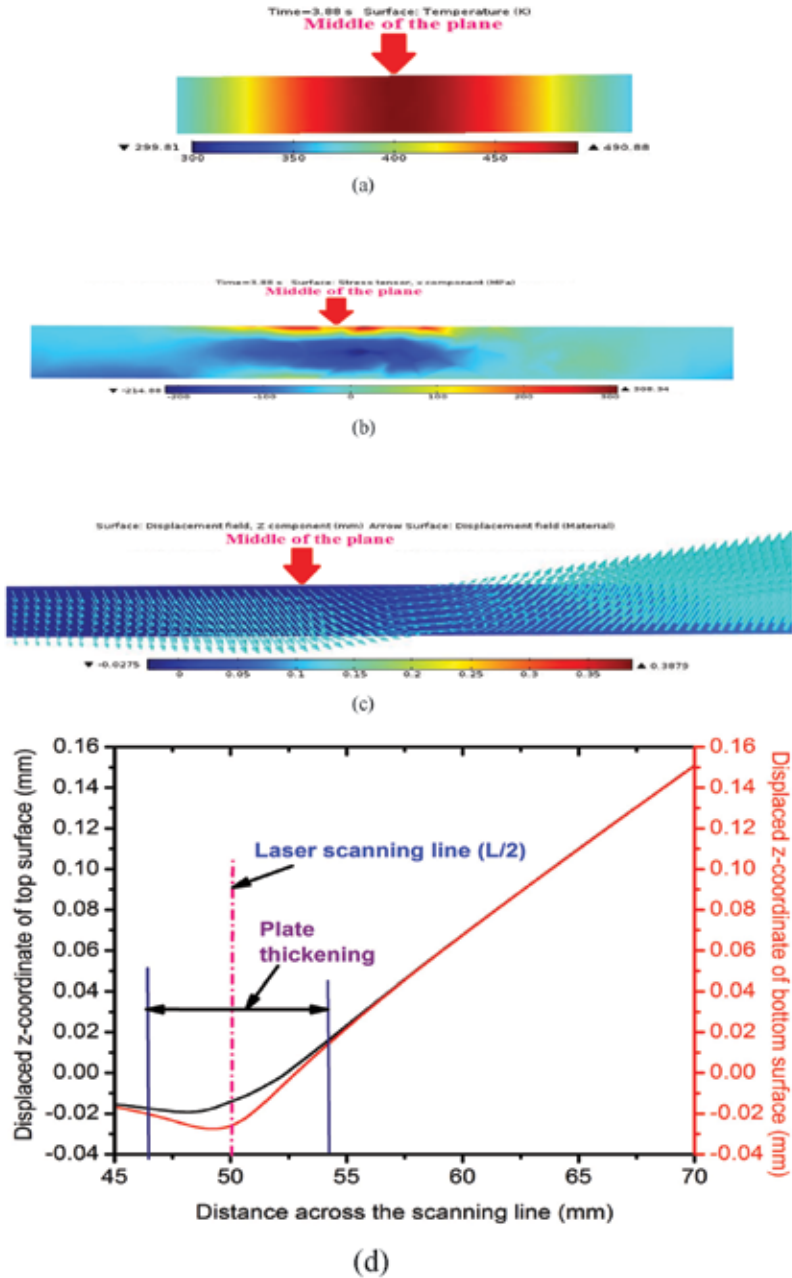


FIGURE 21

Images showing (a) temperature distribution, (b) x -component of stress, (c) z -component of displacement with nodal displacement vector and (d) a graph showing displacement across the scanning line on the X-Z plane at $t=3.88$ seconds.

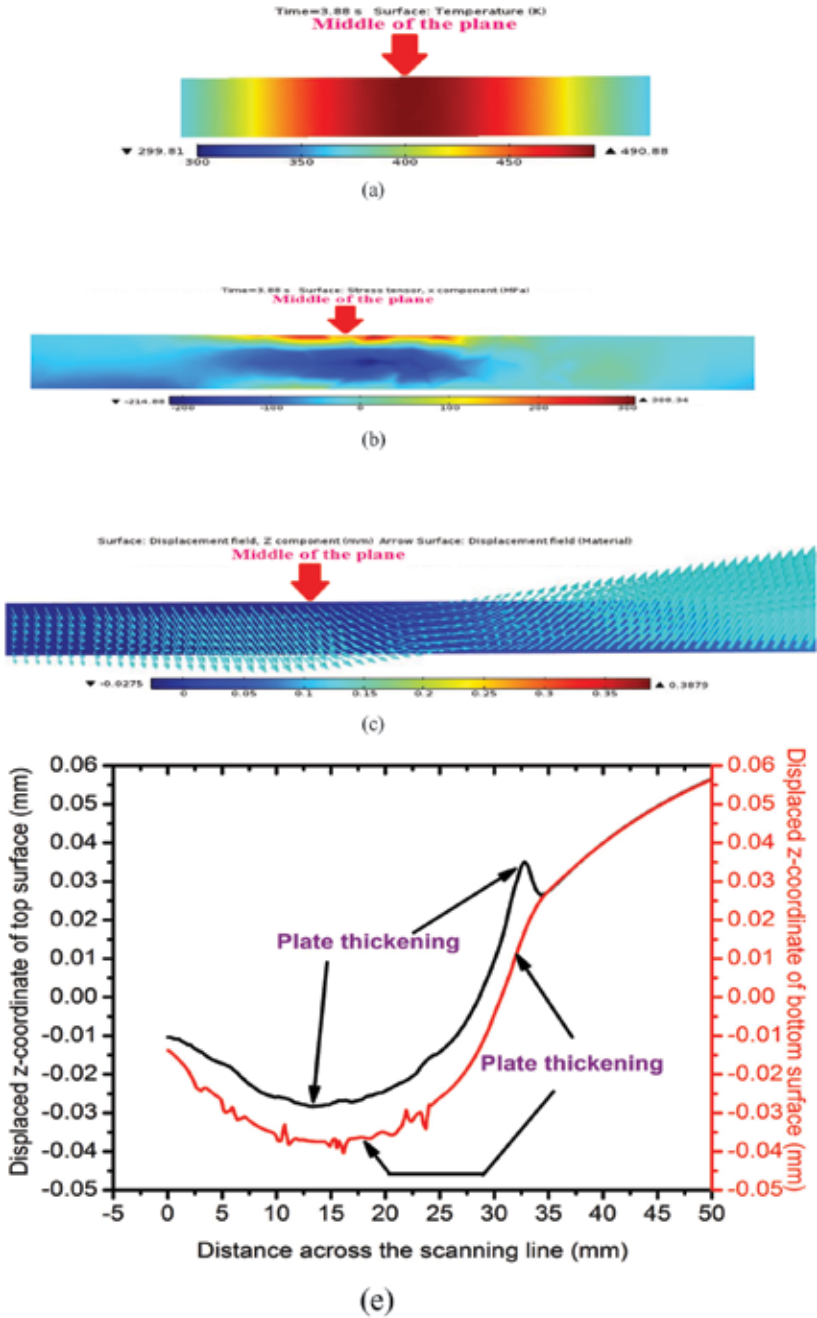


FIGURE 22 Images showing (a) temperature distribution, (b) x-component of stress, (c) y-component of stress, (d) z-component of displacement with nodal displacement vector and (e) a graph showing displacement across the scanning line on the Y-Z plane at $t=3.88$ seconds.

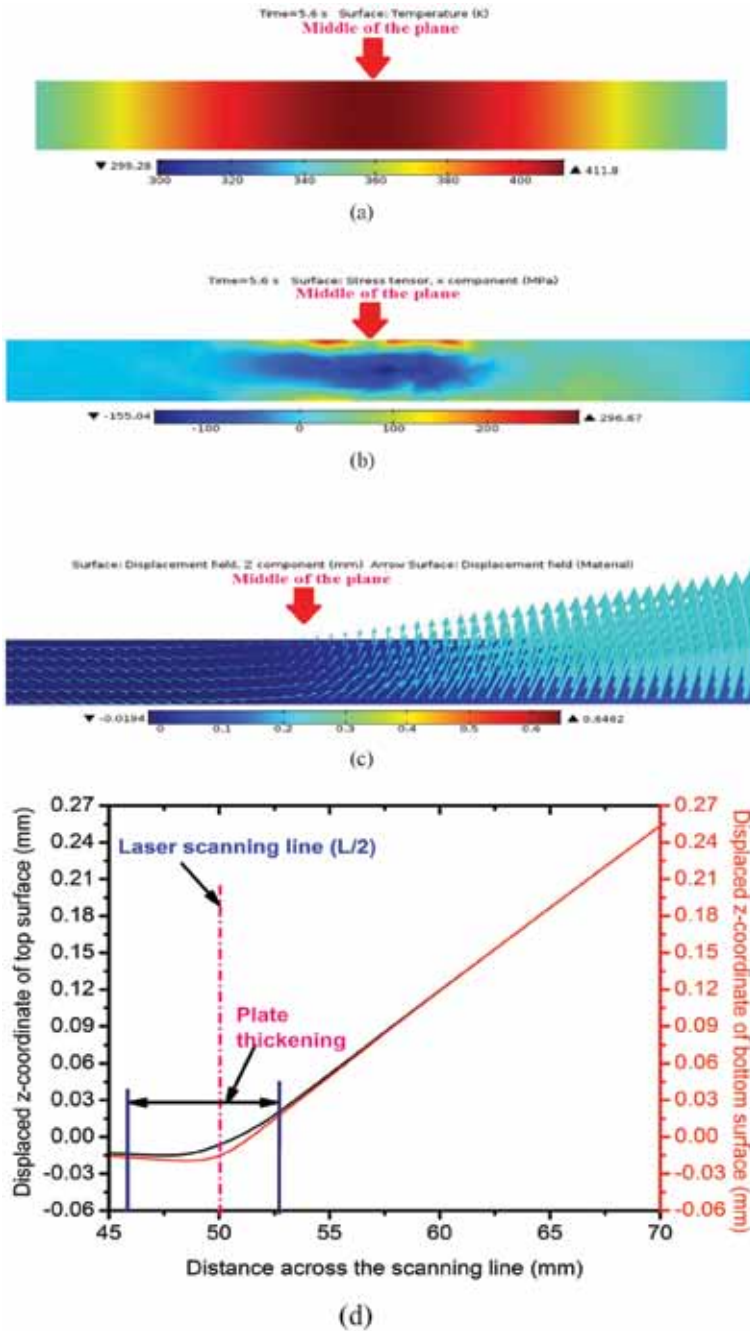


FIGURE 23

Images showing (a) temperature distribution, (b) x -component of stress, (c) z -component of displacement with nodal displacement vector and (d) a graph showing displacement across the scanning line on the X-Z plane at $t=5.60$ seconds.

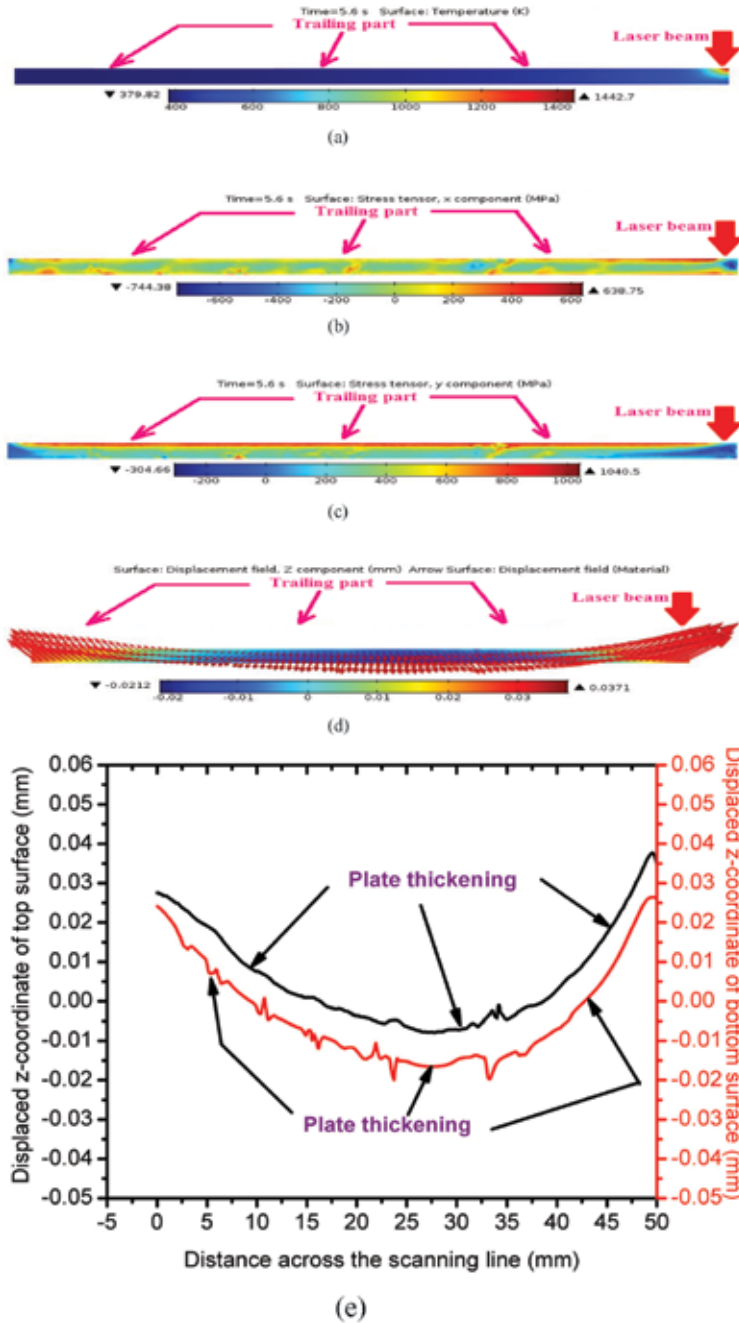


FIGURE 24

Images showing (a) temperature distribution, (b) x-component of stress, (c) y-component of stress, (d) z-component of displacement with nodal displacement vector and (e) a graph showing displacement across the scanning line on the Y-Z plane at t=5.60 seconds.

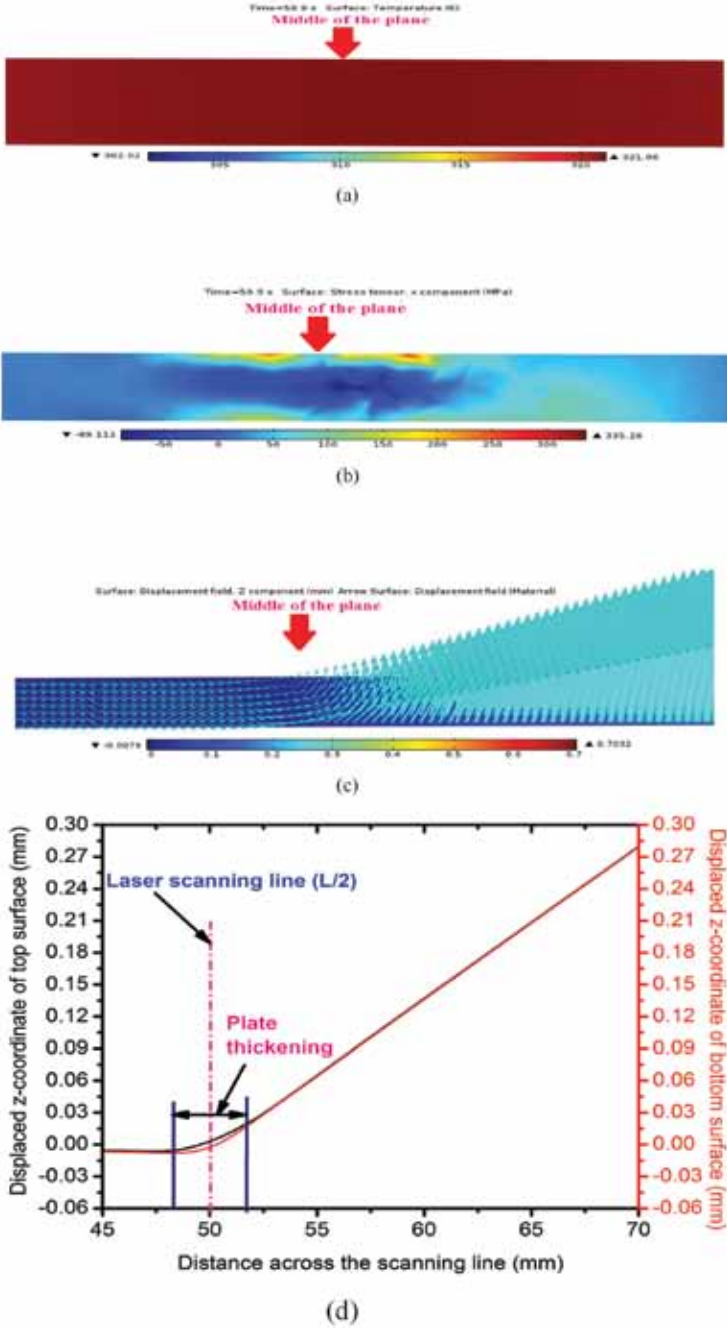


FIGURE 25

Images showing (a) temperature distribution, (b) x-component of stress, (c) z-component of displacement with nodal displacement vector and (d) a graph showing displacement across the scanning line on the X-Z plane at t=59.90 seconds.

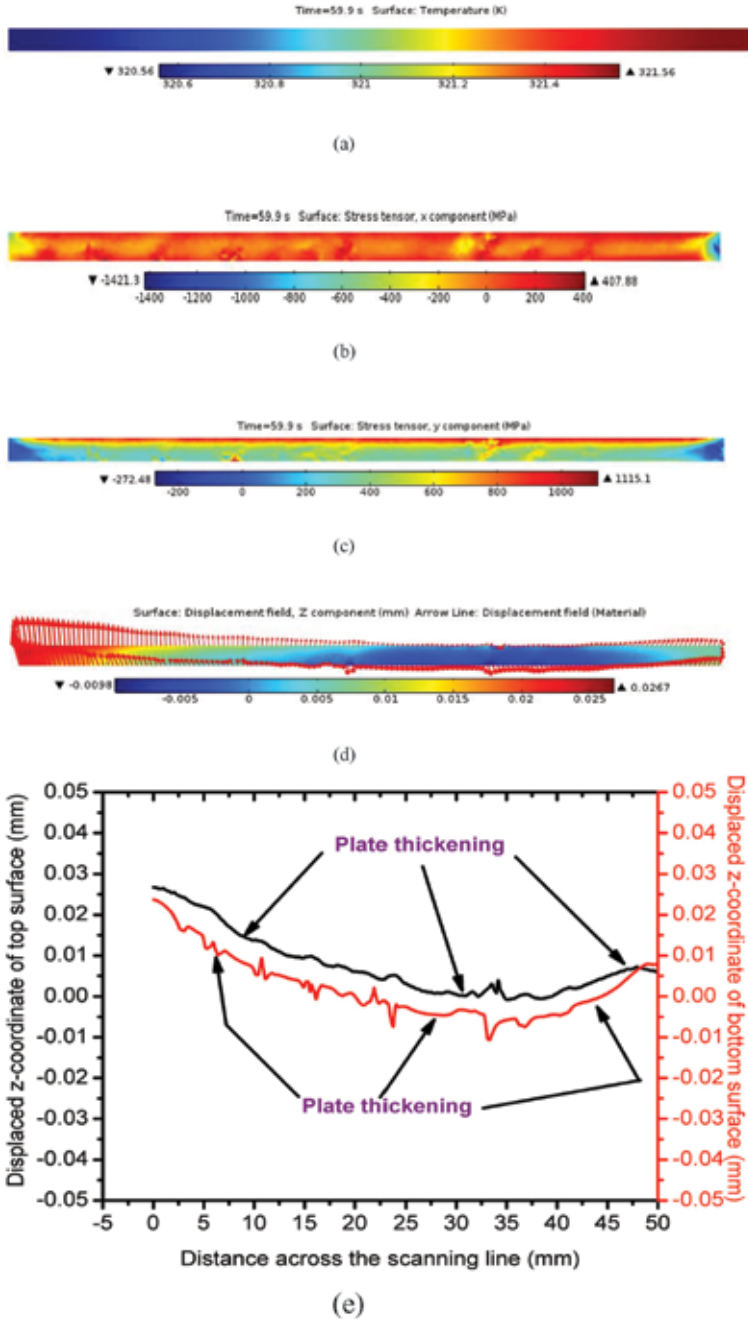


FIGURE 26

Images showing (a) temperature distribution, (b) x-component of stress, (c) y-component of stress, (d) z-component of displacement with nodal displacement vector and (e) a graph showing displacement across the scanning line on the Y-Z plane at $t=59.90$ seconds.

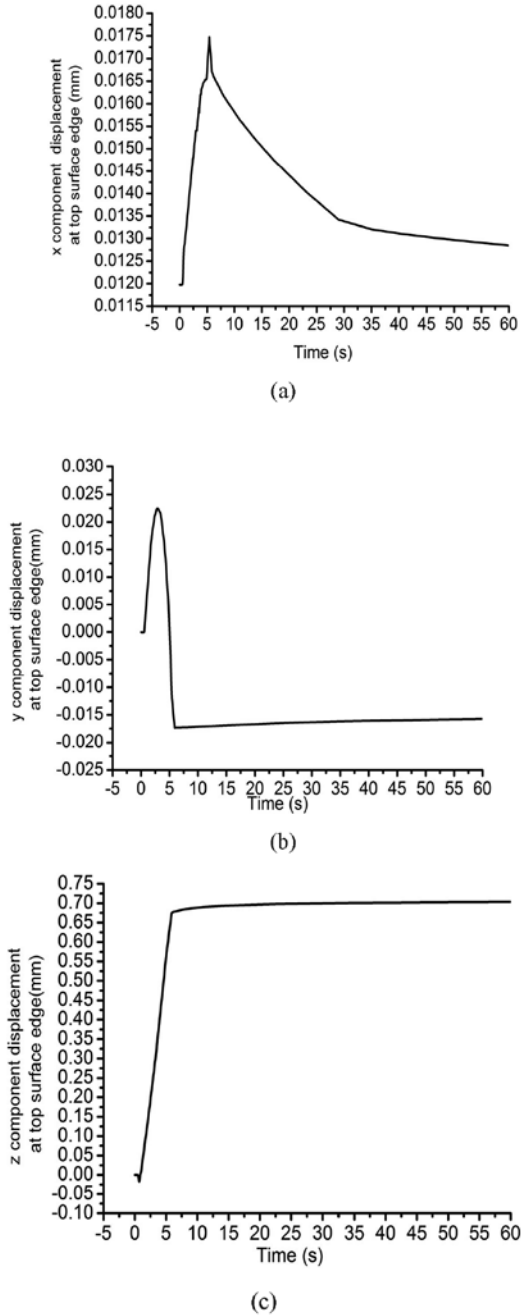


FIGURE 27

Graphs showing the displacement at different components at the top surface of the plate edge: (a) x -component of displacement; (b) y -component of displacement; and (c) z -component of displacement.

ing heating, peak temperature is attained at the farthest point on the scanning line. Later, the temperature starts to drop once laser beam leaves the plate, as shown in Figure 26(a). It can be seen from Figure 26(a) that after cooling, the temperature drops to near ambient along Y-Z plane of the plate at t approximately 60 seconds.

3.14 Plate geometry changes at the plate free edge

To observe the plate geometry changes when the laser beam is irradiating along the mid-length of the plate, the variation of x -component of displacement with time at a point having a coordinate (100.0, 25.0, 1.5) on the plate free edge top surface is monitored and shown in Figure 27(a). Similarly, the variation of y - and z -component of displacements are monitored with time at the same coordinate as shown in Figure 27(b) and Figure 27(c).

From Figure 27(a) it can be seen that the dimension of the plate increases in the plate length direction (+ve X-axis). The reason for this is that during heating process the solid particles in the plate will heat up and it does expand by thermal expansion. Once the heat which has been given to the plate is dissipated, the plate dimension starts to decline due to contraction, as shown in Figure 27(a). From Figure 27(b) it can be seen that the plate moving towards to the laser scanning direction (+ve Y-axis) until the laser beam irradiates the half width of the plate. Afterwards, the plate starts to move in opposite direction to the laser scanning direction (-ve Y-axis) during rest of the heating. During the cooling phase, the plate moves towards to the laser scanning direction (+ve Y-axis) with very slow rate due to contraction. Figure 27(c) shows the variation of z -component of displacement with time during the heating and cooling process. It can be seen from the figure that the z -component of displacement increases during the laser heating process and remains fixed during the cooling time.

4 CONCLUSIONS

A finite element (FE) model for the laser forming process of AISI 304 stainless steel is carried out to gain greater understanding of the mechanism of laser forming process. The temperature, stress and displacement distributions are captured at every time interval from the simulation on the two cross-sections of the plate. The plate behaviour during the laser bending process has been stated during three vital stages: (i) at the early stage of heating; (ii) at the intermediate portion of the plate; and (iii) the farthest edge of the plate and during the cooling phase. The plate thickening along the scanning line produced by laser irradiation and the plate geometry changes on the plate free edge top surface have also been demonstrated.

REFERENCES

- [1] Vollertsen F. Mechanisms and model for laser forming. *Laser Assisted Net Shape Engineering : Proceedings of the 26th International CIRP Seminar on Manufacturing Systems - LANE '94*. 12-14 October 1994, Erlangen, Germany. **1**, 345-360.
- [2] Geiger M. and Vollertsen F. Mechanisms of laser forming. *CIRP Annals* **42**(1) (1993), 301-304.
- [3] Marya M. and Edwards G.R. Factors affecting the laser bending of Ti-6Al-2Sn-4Zr-2Mo. *Journal of Laser Applications* **12**(4) (2000), 149-159.
- [4] Vollertsen F., Komel I. and Kals R. The laser bending of steel foils for micro-parts by the buckling mechanism - A model. *Modeling and Simulation in Material Science & Engineering* **3**(1) (1995), 107-119.
- [5] Wu D., Ma G., Niu F. and Guo D. Temperature gradient mechanism on laser bending of borosilicate glass sheet. *Journal of Manufacturing Science and Engineering* **132**(1) (2010), 011013-6.
- [6] Che Jamil M.S., Sheikh M.A. and Li L. A finite element study of buckling and upsetting mechanisms in laser forming of plates and tubes. *International Journal of Manufacturing, Materials, and Mechanical Engineering* **1**(1) (2011), 1-17.
- [7] Li W. and Yao Y.L. Laser bending of tubes: mechanism, analysis, and prediction. *Journal of Manufacturing Science and Engineering* **123**(4) (2001), 674-681.
- [8] Chen G. and Zhang P. Laser micro bending process of Ti6Al4V square bar. *Micromachines* **5**(2) (2014), 359-372.
- [9] Pence C., Ding H., Shen N-G. and Ding H-T. Experimental analysis of sheet metal micro-bending using a nanosecond-pulsed laser. *International Journal of Advanced Manufacturing Technology* **69**(1-4) (2013), 319-327.
- [10] Che Jamil M.S., Sheikh M.A. and Li L. A numerical study of the temperature gradient mechanism in laser forming using different laser beam geometries. *Lasers in Engineering* **22**(5-6) (2011), 413-428.
- [11] Lawrence J., Schmidt M.J.J. and Li L. The forming of EN3 mild steel plates with a 2.5 kW high power diode laser. *International Journal of Machine Tools and Manufacture: Design Research and Application* **41**(7) (2001), 967-977.
- [12] Shen. Mechanism of laser micro-adjustment. *Journal of Physics D: Applied Physics* **41**(24) (2008), 1-9.
- [13] Shi Y., Shen H., Yao Z. and Hu J. Temperature gradient mechanism in laser forming of thin plates. *Optics & Laser Technology* **39**(4) (2007), 858-863.
- [14] Shi Y., Liu Y., Yao Z. and Shen H. A study on bending direction of sheet metal in laser forming. *Journal of Applied Physics* **103**(5) (2008), 053101-6.
- [15] Paramasivan K., Das S. and Misra D. A study on the effect of rectangular cut out on laser forming of AISI 304 plates. *International Journal of Advanced Manufacturing Technology* **72**(9-12) (2014), 1513-1525.